LA-UR-14-28482
Approved for public release; distribution is unlimited.

Title: Technical Report on the Status of Nonlinear Ultrasonic Techniques for Non-Destructive Inspection

Author(s):
Anderson, Brian Eric
Remillieux, Marcel
Haupert, Sylvain
Ohara, Yoshikazu
Lake, Colton R.
Ulrich, Timothy James II

Intended for: Report

Issued: 2014-10-31

APPENDIX E

FCT DOCUMENT COVER SHEET [1]

Name/Title of Deliverable/Milestone/Revision No.	M3FT-14LA0802031 Technical Report on the Status of Nonlinear Ultrasonic Techniques for Non-Destructive Inspection
Work Package Title and Number	FT-14LA080203 Field Demonstration Support - LANL
Work Package WBS Number	1.02.08.02
Responsible Work Package Manager	TJ Ulrich Digitally signed by TJ Ulrich DN: cn=TJ Ulrich, o=LANL, ou=EES-17, email=tju@lanl.gov, c=US Date: 2014.09.18 12:20:38 -06'00' (Name/Signature)
Date Submitted	

Quality Rigor Level for Deliverable/Milestone[2]	☒ QRL-3	☐ QRL-2	☐ QRL-1 ☐ Nuclear Data	☐ Lab/Participant QA Program (no additional FCT QA requirements)

This deliverable was prepared in accordance with Los Alamos National Laboratory
(Participant/National Laboratory Name)

QA program which meets the requirements of
☒ DOE Order 414.1 ☐ NQA-1-2000 ☐ Other

This Deliverable was subjected to:

☒ Technical Review ☐ Peer Review

Technical Review (TR)	**Peer Review (PR)**
Review Documentation Provided	**Review Documentation Provided**
☐ Signed TR Report or,	☐ Signed PR Report or,
☐ Signed TR Concurrence Sheet or,	☐ Signed PR Concurrence Sheet or,
☒ Signature of TR Reviewer(s) below	☐ Signature of PR Reviewer(s) below

Name and Signature of Reviewers

James Ten Cate Digitally signed by James Ten Cate DN: cn=James Ten Cate, o=LANS, ou, email=tencate@lanl.gov, c=US Date: 2014.09.18 14:02:43 -06'00'	
Pierre-Yves Le Bas Digitally signed by Pierre-Yves Le Bas DN: cn=Pierre-Yves Le Bas, o, ou=EES-17, email=pylb@lanl.gov, c=US Date: 2014.09.18 14:06:31 -06'00'	

NOTE 1: *Appendix E should be filled out and submitted with the deliverable. Or, if the PICS:NE system permits, completely enter all applicable information in the PICS:NE Deliverable Form. The requirement is to ensure that all applicable information is entered either in the PICS:NE system or by using the FCT Document Cover Sheet.*

NOTE 2: *In some cases there may be a milestone where an item is being fabricated, maintenance is being performed on a facility, or a document is being issued through a formal document control process where it specifically calls out a formal review of the document. In these cases, documentation (e.g., inspection report, maintenance request, work planning package documentation or the documented review of the issued document through the document control process) of the completion of the activity, along with the Document Cover Sheet, is sufficient to demonstrate achieving the milestone. If QRL 1, 2, or 3 is not assigned, then the Lab / Participant QA Program (no additional FCT QA requirements) box must be checked, and the work is understood to be performed and any deliverable developed in conformance with the respective National Laboratory / Participant, DOE or NNSA-approved QA Program.*

Technical Report on the Status of Nonlinear Ultrasonic Techniques for Non-Destructive Inspection

Fuel Cycle Research & Development

Prepared for
U.S. Department of Energy
Used Fuel Campaign
B.E. Anderson, M. Remillieux, S. Haupert, Y. Ohara, P. Shokouhi, C. Lake, and T.J. Ulrich
Los Alamos National Laboratory
18 September 2014
FCRD-UFD-2014-000307

SUMMARY

This report summarizes technical work conducted by LANL staff and international collaborators in support of the UFD Storage Experimentation effort. The overall focus of this technical work is two-fold: a) on the detection and imaging of a failure mechanism known as stress corrosion cracking (SCC) in stainless steel, and b) on evaluating concrete degradation using nonlinear ultrasonic techniques. This year we report here on three research efforts: 1) experimental effort utilizing TREND and SPACE inspection techniques for crack detection in stainless steel; 2) numerical modeling of 3D time reversal focusing to quantify TREND inspection regions; and 3) application of nonlinear ultrasonic techniques for quantifying concrete degradation. The first and third were collaborative efforts. The first was performed in conjunction with the Tohoku University (Sendai, Japan) and CNRS Parametric Imaging Laboratory (Laboratoire d'Imagerie Parametrique, in Paris, France), with support from the Electricity of France (Électricité de France, [EDF], in Paris, France) project. The third research effort was performed in conjunction with the Federal Institute for Material Research and Testing (Bundesanstalt für Materialforschung und –prüfung, in Berlin, Germany) and The Pennsylvania State University (State College, PA). The conclusion to be made from these results is that nonlinear ultrasound is applicable as a spot inspection technique in both stainless steel and concrete, with the potential to be more broadly applied to other materials and environments. The nonlinear signature measured is related to the degree of damage/degradation. The localized nature of the measurement allows for identification of mechanical defects and localization of degraded regions. Further work is necessary to characterize the degradation (e.g., sensitivity, size of flaws, type of damage, residual strength, etc.). Additionally, for the SCC work to continue to progress, relevant samples must be acquired for study.

CONTENTS

FIGURES

TABLES

ACRONYMS

AISI	American Iron and Steel Institute
BAM	the Federal Institute for Material Research and Testing (Bundesanstalt für Materialforschung und –prüfung, Germany)
CC	Chaotic Cavity
CNRS	Centre National de la Recherche Scientifique (France)
COMSOL	A commercial, finite element solver and simulation package
CWI	Coda Wave Interferometry
DAE(T)	Dynamic Acousto-Elasticity (Technique)
EDF	Electricity of France (Électricité de France)
GE	General Electric
IR	Impulse Response
LANL	Los Alamos National Laboratory
LDV	Laser Doppler Vibrometer
MTS	Company that provides compression testing equipment
NDT	Nondestructive Testing
NEWS	Nonlinear Elastic Wave Spectroscopy
NLUT	Nonlinear Ultrasonic Techniques
NRUS	Nonlinear Resonant Ultrasound Spectroscopy
PZT	Lead Zirconate Titanate (transducer)
RITA	Resonance Inspection Techniques and Analysis
ROI	Region of Interest
RUS	Resonant Ultrasound Spectroscopy
SAW	Surface Acoustic Wave
SCC	Stress Corrosion Cracking
SPACE	Sub-harmonic Phased Array for Crack Evaluation
SSM	Scaling Subtraction Method
TOF	Time of Flight
TR	Time Reversal
TREND	Time Reversal Elastic Nonlinearity Diagnostic

USED FUEL DISPOSITION CAMPAIGN / STORAGE & TRANSPORTATION EXPERIMENTS PROGRAM

1. Introduction

This document describes the technical work dealing with the determination of the potential use of nonlinear elastic wave spectroscopy (NEWS) and other nonlinear ultrasonic techniques (NLUT) for detection, monitoring, characterization and imaging of material degradation in materials relevant to the storage of used nuclear fuel. Particular importance has been placed upon stress corrosion cracking (SCC) of stainless steel and various degradation mechanisms of concrete due to the ubiquity of these materials in nuclear fuel storage facilities. We report here on three research efforts: 1) experimental effort utilizing TREND and SPACE inspection techniques for crack detection in stainless steel; 2) numerical modeling of 3D time reversal focusing to quantify TREND inspection regions; and 3) experimental application of nonlinear ultrasonic techniques for quantifying concrete degradation. The first was performed in conjunction with the Tohoku University (Sendai, Japan) and CNRS Parametric Imaging Laboratory (Laboratoire d'Imagerie Parametrique, in Paris, France), with support from the Electricity of France (Électricité de France, [EDF], in Paris, France) project. The third research effort was performed in conjunction with the Federal Institute for Material Research and Testing (Bundesanstalt für Materialforschung und –prüfung, in Berlin, Germany) and The Pennsylvania State University (State College, PA).

2. SCC Detection and Imaging

Austenitic stainless steels are known to be susceptible to stress corrosion cracking (SCC), which is an aggressive type of corrosion that exists when a material under tensile stress is placed in a corrosive environment [1]. This is of particular concern as the processing (i.e., cold rolling) and construction (welding) of storage canisters produce an inherent residual stress in metals that can lead to SCC, therefore our goal is to study the formation of stress corrosion cracks within Type 304L stainless steel, which is frequently used in containers for used nuclear fuel disposal. The conditions present in storage canisters (i.e., elevated temperatures, high residual stresses near welds and exposure to salt water/vapor) make them susceptible to SCC potentially leading to critical through-wall failure, and thus loss of containment [2]. The timescales on which through-wall failure is expected in a storage canister under typical conditions is on the order of 10's of years. While through-wall flaws are catastrophic, the long timescales allow for routine inspection, and potentially mitigation, providing methods exist. The following study is focused on the former problem, i.e. detection of SCC, and thus the development of a tool for inspection of storage canisters.

2.1 Closed and Open Cracks

Closed and open cracks both present potential catastrophic failure mechanisms. The difference between these types of cracks is whether or not the opposing crack surfaces are in contact with each other. Larger cracks tend to be open (crack surfaces are separated) while newly forming cracks are typically closed, i.e., opposing crack surfaces are in direct contact. Traditional acoustic techniques typically rely on the detection of an echo of sound reflecting off of a crack surface. Thus traditional techniques do not have the ability to detect closed cracks since the incident sound waves pass through a closed crack without a significant echo. Fortunately closed cracks have been shown to be visible to nonlinear ultrasound techniques [3]. In this report we refer to traditional acoustic techniques as being linear techniques that have been shown to image open cracks, whereas we'll refer to nonlinear acoustic techniques, including TREND, as those known to image closed cracks.

2.2 The Time Reversed Elastic Nonlinearity Diagnostic (TREND)

Time reversal (TR) is a method that allows one to focus wave energy to a specific location in space [4]. The ability of TR to create a highly localized focus of energy provides the ability to interrogate the properties of a specific location in space. When closed cracks and cracks with small openings (i.e., surfaces separated by distances less than the imposed vibrational strain) vibrate they do so nonlinearly, meaning they exhibit vibrational distortions of the excitation thus vibrating at frequencies not present in the source of the excitation (e.g., ultrasonic probe). Open cracks act as voids and thus respond linearly, or without the aforementioned distortions [5]. Detecting nonlinearities is easier at higher amplitudes due to (a) the amplitude dependence of the nonlinear response and b) a higher signal to noise at frequencies of interest (e.g. harmonic frequencies, sum and difference frequencies, etc.). The time reversed elastic nonlinearity diagnostic (TREND) [6] [7] is a protocol where one creates a TR focus at one or more locations within a region of interest (ROI) and the resulting focal signals are analyzed for a nonlinear elastic response. TREND has been used to image surficial and near-surficial nonlinear features in solid samples [7] [8].

Various physics-based techniques can be used to quantify the nonlinearity at each point in a ROI and thus allow crack localization and potentially characterization. The scaling subtraction method (SSM) is one such technique that may be used in a time reversal experiment by creating a low amplitude TR focus and a high amplitude TR focus at a specific location of interest, scaling the low amplitude signal, and then subtracting the scaled low amplitude signal from the high amplitude signal and integrating the squared signal over a given time window [9]. It should be noted that many signal processing techniques have been developed to quantify the nonlinear response. SSM has been selected here due to the ease of application and the lack of any need for complex computations. Other analysis techniques may also be explored in the future to enhance the sensitivity.

2.3 Subharmonic Phased Array for Crack Evaluation (SPACE)

Tohoku University in Sendai, Japan has developed a phased array acoustic technique to image cracks. A phased array broadcasts a coherent acoustic energy beam along a certain direction and listens for reflected energy signatures [10] [11]. In the case of SPACE [12] [13] [14], the phased array emits energy at one frequency, the fundamental, and listens for reflections at both the fundamental frequency and half of that original frequency, i.e., the subharmonic. This allows for traditional ultrasonic reflection imaging (using the fundamental) as well as nonlinear imaging (using the subharmonic.) The angle of the reflected energy indicates the direction in which the crack lies and the timing of the reflected energy yields range information as to its location. SPACE has been demonstrated to image linear, open cracks through the information contained at the original frequency and to be able to image nonlinear, closed crack through the information contained at half of the original frequency.

There are two versions of SPACE techniques. Bulk-SPACE transmits sound energy into the bulk of the sample and is limited to imaging cracks that are subsurface. As a result Bulk-SPACE is used to image cracks located on one side of a plate like sample, while the array is located on the opposite side of the plate. Practically, this means that Bulk-SPACE is able to image cracks on the internal surface of a cask, but not on the exterior surface. A new type of SPACE technique is being developed that utilizes surface acoustic waves (SAW). SAW-SPACE transmits energy along the same surface as the array hardware, thus enabling the ability to detect surficial features. Being restricted to the use of SAW, however, removes the ability to detect the subsurface features. A combination of Bulk and SAW SPACE would be necessary to detect cracks in all regions (i.e., surface and subsurface.)

2.4 Collaborative Research on EDF Samples

One of the biggest challenges facing the further development of SCC imaging is obtaining realistic samples that either contain SCC or contain closed cracks generated through some other means. Previous research conducted at LANL has utilized a sample that was obtained from General Electric (GE) by way of Sandia National Laboratories. This sample has examples of SCC, however, these cracks were created under extreme loading conditions resulting in large open cracks that are not representative of the expected SCC. Samples with less developed SCC are needed. A collaboration has been developed with Tohoku University (in Sendai, Japan) and Electricity of France (EDF in Paris, France). In this effort EDF has agreed to provide samples for LANL and for Tohoku to test various ultrasonic techniques and compare the performance of TREND and SPACE techniques. EDF obtained samples from Trueflaw (in Espoo, Finland) and sent the first sample to LANL for preliminary TREND testing. This sample, along with two additional samples from Trueflaw, were examined using SPACE at Tohoku. Experiments on all three samples are planned for FY15 LANL using TREND.

2.4.1 Samples Provided by EDF

EDF obtained three samples manufactured by Trueflaw [15]. The cracks were produced in-situ with controlled thermal fatigue loading. The crack was grown using a natural thermal fatigue damage mechanism. The samples are all austenitic stainless steel AISI 304. Information on the cracks produced in each sample is provided in Table 1.

Table 1. Samples and crack dimensions as provided by TrueFlaw.

	Length (mm)	Depth (mm)	Surface Thickness (μm)*	Sample Dimensions (mm)
EDFsample01	5.3	1.9	5	150x100x20
EDFsample02	5.9	1.9	14	150x100x60
EDFsample03	12.0	4.9	31.5	150x100x60

**Surface thickness measured by optical microscopy at Tohoku, other dimensions provided by Trueflaw.*

2.4.2 Linear Phased Array Measurements on EDF Samples

Linear phased array measurements were performed on each EDF sample in order to 1) determine whether the crack has a linear response (i.e., corresponds to an open crack); 2) determine the open crack length at the surface; and 3) determine whether the crack tip produced an echo to estimate the crack depth. The measurements were performed along each side of the crack with an image taken at 1 mm steps. The probe is a 32 element array with a 5 MHz center frequency. This information was extracted from the phased array image intensity. The length of the crack is determined by use of the points at half the max intensity on either end of the crack. The width of the probe is 22 mm and thus the acoustic beam has a finite width resulting in an approximate determination of the crack length. It was found that all three of the cracks returned an echo signal, meaning that at least a portion of each crack is open. It was possible to image the crack tip with the first sample and in one scan of the third sample but not in the other scan of this sample. Figures 1 and 2 show schematic drawings of the measurements and sample phased array measurements, respectively. In general the phased array measurements found the open length of the crack opening to be 30% longer than the measurements provided by Trueflaw.

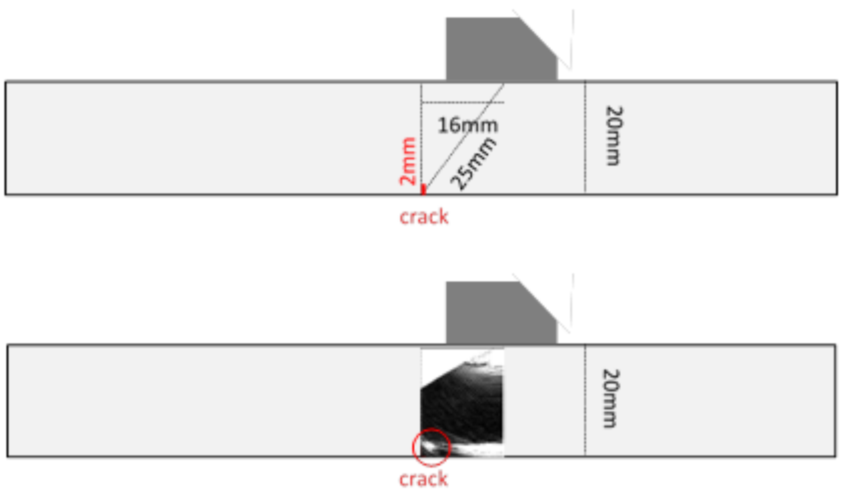

Figure 1. Schematic drawing of the array probe (dark grey) placed on a sample to image the crack from an angle, along with a sample phased array image showing the reflection of sound off of the crack opening (in white.)

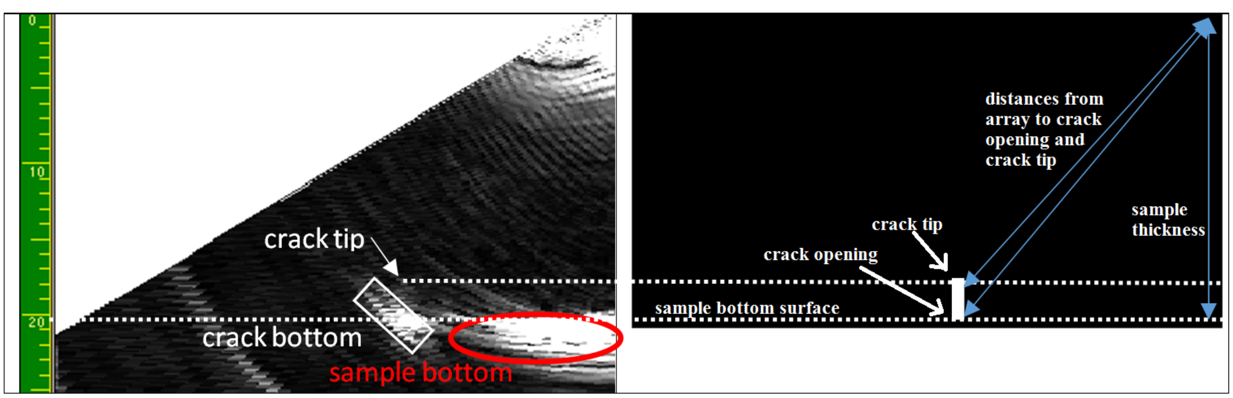

Figure 2. Sample phased array image showing the intensity of the recorded sound reflections in a black to white scale (white being higher intensity). The bottom surface was always clearly visible and the probe had to be oriented to see the crack opening as a separate image from the bottom image. In some cases the crack tip was just visible as shown above.

2.4.3 Bulk-SPACE Measurements on EDF Samples

As described previously, Bulk-SPACE measurements are ideal for imaging cracks on the opposing side of the phased array, i.e., probing interior surfaces from external access [12] [13] [14]. The probe used for this study is the same as that used for the linear phased array measurements. In these measurements, the phased array is used to focus the incident energy at several specified depths and angles. These parameters were determined according to the sample under test. For the current measurements, a fundamental frequency of 6.9 MHz was emitted, meaning that the principle subharmonic energy would be detected at 3.45 MHz. The probe was oriented perpendicular to the crack. The probe was positioned at various locations along the length of the crack at 1 mm or 2 mm steps depending on the particular setup.

Beam forming and signal processing are performed on the waveform signals acquired at each measurement position. The final result consists of two matrices. The first matrix contains the maximum amplitude at the fundamental frequency, while the second matrix contains the maximum of the subharmonic frequency. The values from both matrices are utilized with the same image processing as for the linear phased array in order to remove ghosts and artifacts from the images. Sample results showing the higher subharmonic intensity, among the measurement scan positions, are presented for each sample in Fig. 3.

In Fig. 3, we can observe that the echoes are larger in case of the subharmonic frequency images than for the fundamental images for samples 2 and 3. Moreover, there is a different pattern for the subharmonic image and fundamental image. In the case of sample 1, the fundamental image shows a single spot (i.e., echo) corresponding to the bottom of the crack while the subharmonic image shows a dipole-like response with two lobes. In the case of sample 2, an echo is visible in the subharmonic image while there is no echo for the fundamental, irrespective of the position of the probe (left or right side of the crack). Finally, in the case of sample 3, the fundamental image clearly shows two distinct echoes at the crack position while only a single echo is visible in the subharmonic image. No crack tip echo is visible in either the fundamental or subharmonic images.

A quantitative estimation of the crack length is presented in Table 2. One can notice that the crack length is similar for fundamental and subharmonic images. The values are also close to the length given by Trueflaw when the crack echo is visible.

Table 2. Crack length determinations from fundamental and subharmonic images obtained by Bulk-SPACE imaging.

	Crack bottom length (Fundamental)			**Crack bottom length (Subharmonic)**		
	Left side	Right side	average	Left side	Right side	Average
EDFsample01	5	No data	5	5.9	No data	5.9
EDFsample02	Not visible	Not visible	Not visible	9.1	9.2	9.1
EDFsample03	9.5	9.4	9.4	10.6	10.2	10.4

As with the linear phased array technique, the Bulk-SPACE technique is able to detect the crack from the opposite side of the sample. When the nonlinear (i.e., subharmonic image) and linear (i.e., fundamental image) patterns are compared, one can notice that they are different (number and shape of echoes). Moreover the crack is always visible in the subharmonic images while the crack can be missing in the fundamental images (see sample 2). These observations mean that the subharmonic contribution in the signal is not an artifact coming from a leakage of the fundamental contribution but rather is due to a distinct nonlinear source located at the crack position.

In addition to the echo of the crack opening, an echo from the crack tip is expected in the subharmonic images for closed cracks. However, such echoes were not observed. This could be due to the a) crack being open, b) local stress concentrations closing the crack with sufficient force to prevent relative motion of the crack surfaces, or c) the size of the closed portion of the crack falls below the threshold of detection for this technique. Sensitivity studies must be conducted to determine this threshold.

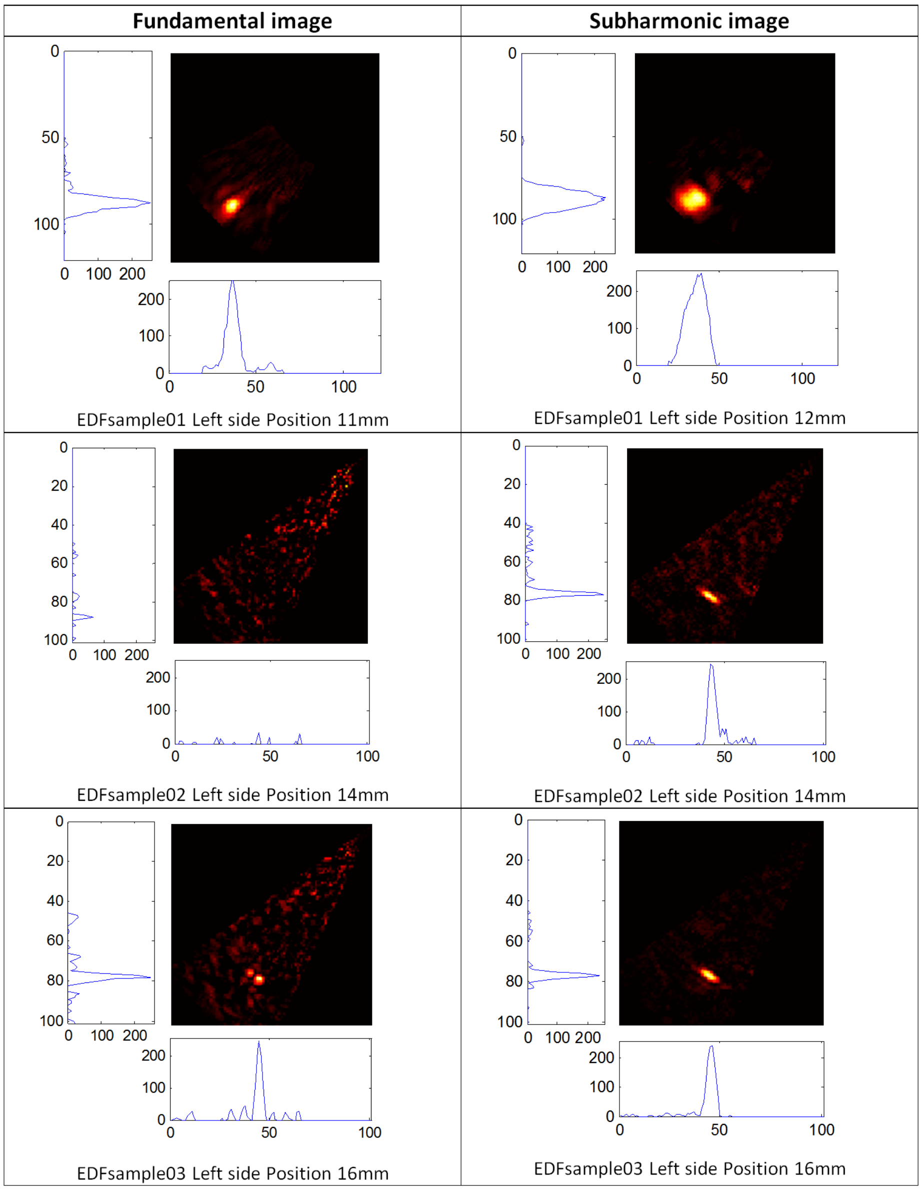

Figure 3. Bulk-SPACE images from each sample at measurement locations where the subharmonic echoes are most visible. The fundamental and subharmonic images are displayed in the left and right columns, respectively. The color scale progresses from black to white.

2.4.4 SAW-SPACE Measurements on EDF Samples

As described previously, SAW-SPACE measurements are ideal for imaging cracks on the inspection surface due to the utilization of surface acoustic waves (Rayleigh waves). For these measurements a 32 element array with a central frequency of 2 MHz was used. For SAW-SPACE measurements, the probe is setup to focus at a single point on the surface 42.6 mm away from the probe (see Fig. 4). The restriction to a single focal position is due to the design of the sensor, which utilizes an angled wedge to optimally generate only surface waves and simultaneously attenuate the propagation of bulk waves into the sample. This restricts the imaging capabilities to the surficial expression of a crack.

The images obtained with the probe parallel to the crack are presented in Fig. 5. One can observe that the nonlinear signatures (i.e. subharmonic image) are very similar to the linear signatures (i.e. fundamental image). The echoes are larger in case of the subharmonic frequency images than for the fundamental. Note that for sample 3, two echoes are visible, in both fundamental and subharmonic images.

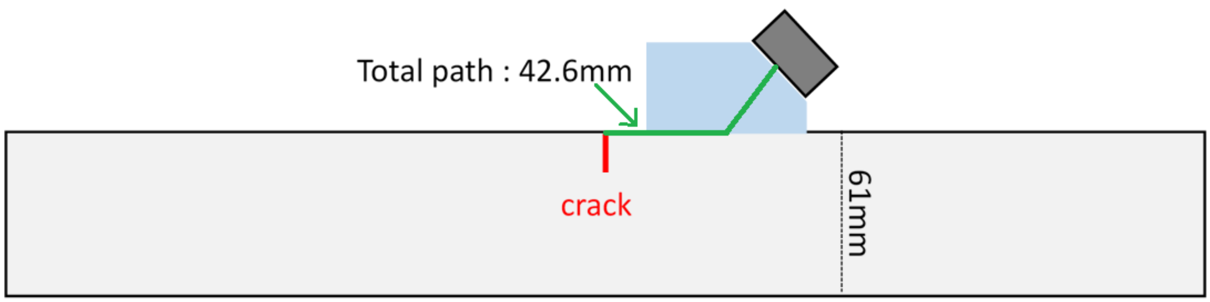

Figure 4. Schematic drawing of a SAW-SPACE measurement performed on sample 1. The total path length that the surface waves travel is 42.6 mm to the focal point at the crack.

The results of a quantitative estimation of the crack length are presented in Table 3. One can notice that the length of the crack opening is similar for the fundamental and subharmonic images. The values are also close to the length given by Trueflaw.

Table 3. Crack bottom length determined on fundamental and subharmonic images obtained by SAW SPACE technique.

	Crack bottom length (Fundamental)			Crack bottom length (Subharmonics)		
	Left side	Right side	average	Left side	Right side	Average
EDFsample01	5.1	5.8	5.4	7.9	6.2	7.0
EDFsample02	4.8	5.9	5.3	6.8	6.9	6.8
EDFsample03	11.2	12.2	11.7	13.8	7.9	10.8

SAW-SPACE is able to detect the crack when the crack is located on the same surface as the probe. When the measurement is performed parallel to the crack, it is possible to estimate the crack length with a good accuracy (the lengths are similar to Trueflaw). Contrary to the Bulk-SPACE results, the fundamental and subharmonic images are similar for SAW-SPACE. The subharmonic images do, however, provide additional information on the extent of the cracks. This indicates that the cracks are predominantly open with closed portions extending from the tip.

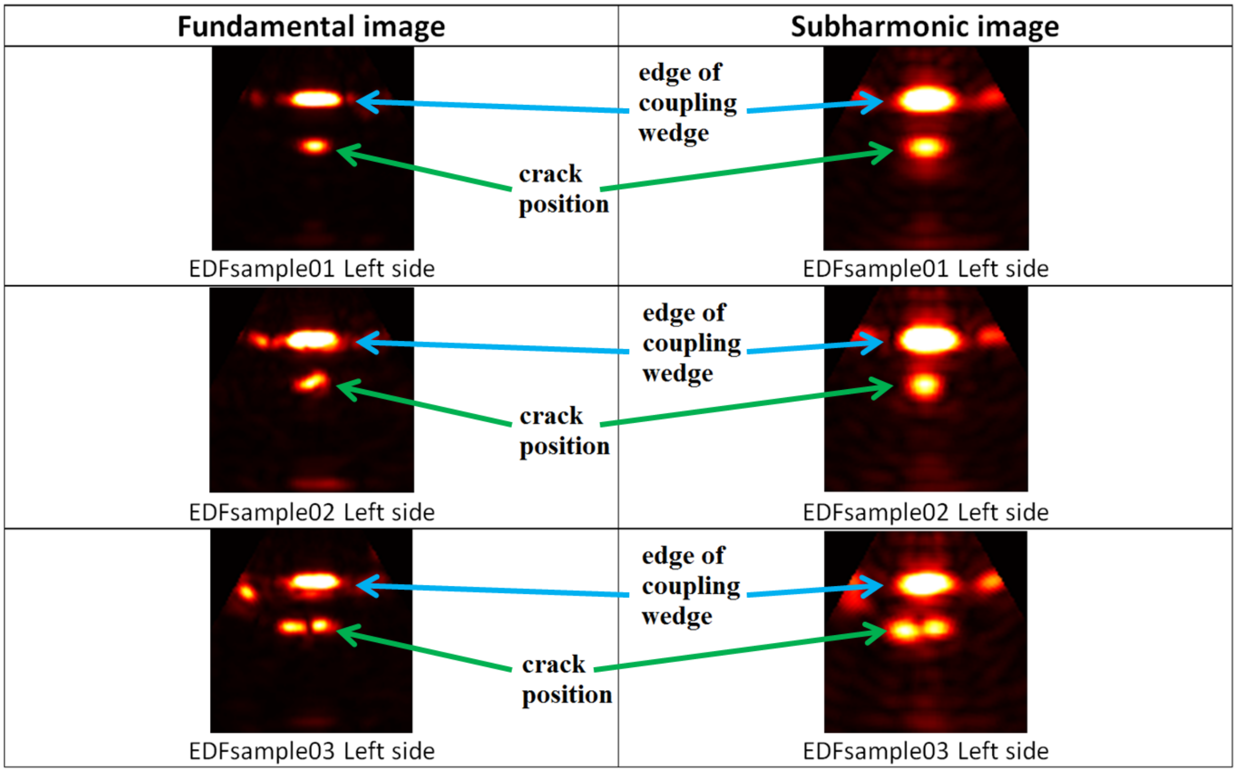

Figure 5. Examples of images that were processed in order to extract the crack length from the fundamental (left column) and subharmonic (right column) images. They correspond to the position where the amplitude of the echo was the maximum.

2.4.5 Preliminary TREND Measurement on One EDF Sample

TREND was used to excite the crack on sample 1. Eight piezoelectric transducers were glued onto an aluminum block of irregular shape (chaotic cavity [CC] [16]) to provide an increase in multiple scattering for the experiment since the amplitude of time reversal focusing is increased when more scattering is used. This CC was then attached to the sample through the use of ultrasound coupling gel. A differential laser vibrometer was used in a configuration to detect in-plane vibrational motion, i.e., parallel to the sample's surface. In-plane motion was oriented perpendicular to the crack in order to maximally excite a clapping mode of the crack, one possible mechanism for the generation of a nonlinear response [17]. The central frequency for the experiment was 80 kHz.

The results of the TREND scans are shown in Fig. 6. These images represent the elastic wave energy present in predetermined narrow frequency bands centered around the fundamental and subharmonic frequencies, respectively. The dashed box in the coarse view of the subharmonic image indicates the ROI used for the fine grid data.

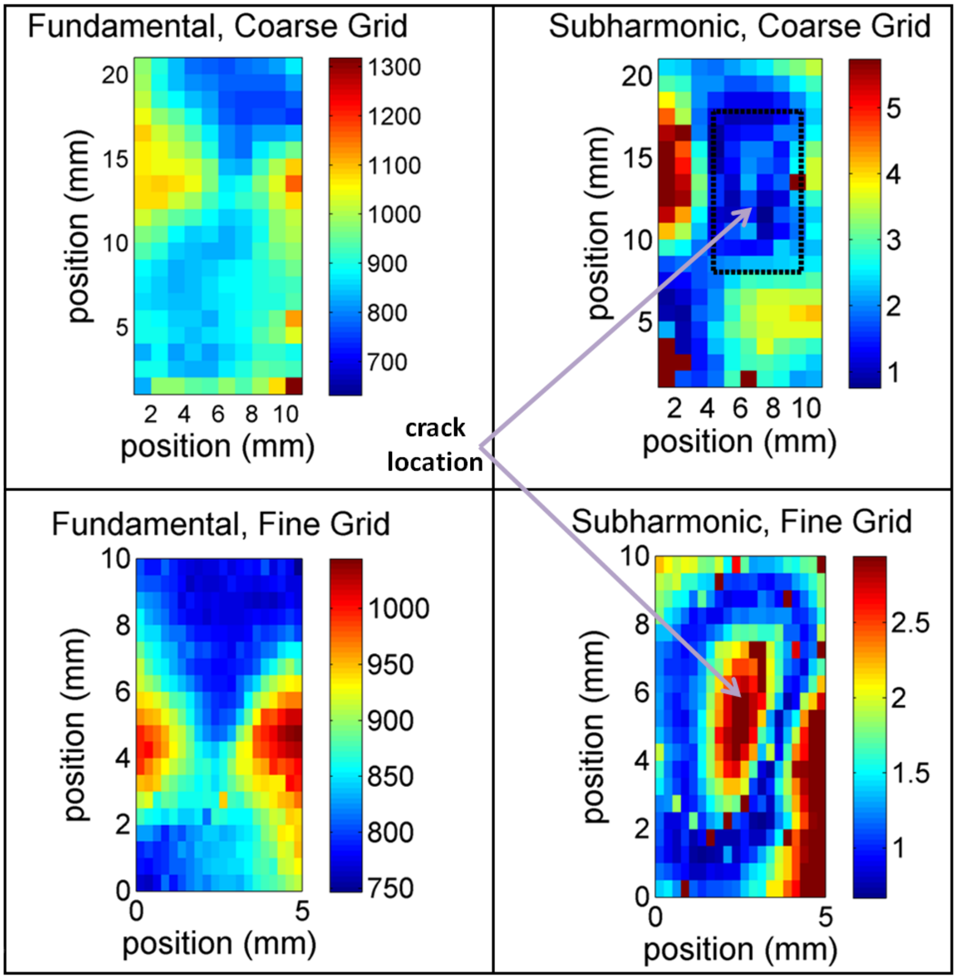

Figure 6. Amplitude of the fundamental and subharmonic components of the TREND focal signals obtained with the in-plane laser vibrometer (orientation being perpendicular to the crack orientation).

A nonlinear feature is clearly seen in the subharmonic fine grid scan at the exact location of the crack. The length of the nonlinear feature is approximately 5mm, matching the length of the crack given by Trueflaw. Note that high amplitude spots are observed outside of the crack region in all of the plots in Fig. 6. These artifacts, likely due to modal responses of the specimen at the excitation frequency, make the detection of the crack more difficult.

This was a first attempt to perform TREND measurements on any of the EDF samples. Further measurements will be conducted in FY15 on all 3 Trueflaw samples. Each sample will be measured using all 3 vibrational components of motion [18] in order to determine the optimal excitation for detection in for both open and closed portions of the crack. Additionally, various frequencies will be used in order to determine penetration depth of the open and close portions of the crack (see Sec. 3.)

2.5 SCC Conclusions and Path Forward

One of the major challenges with developing techniques to image SCC is in obtaining samples that accurately represent SCC. LANL, Tohoku University, CNRS, and EDF have provided resources to collaborate in order to obtain true closed crack samples in order to test the SCC imaging techniques of TREND and SPACE. Three samples provided by EDF, manufactured by Trueflaw, were measured at Tohoku University SPACE techniques, and a preliminary TREND result was obtained at LANL on one of these samples. The evidence collected to date suggests that, despite Trueflaw's assertion that they could provide samples with closed cracks, the samples contain cracks with significant open portions. These original 3 samples will also be tested at LANL with the full range of TREND techniques. EDF will continue to support this effort by providing relevant samples, which is currently a planned activity for FY15.

The linear phased array techniques (linear array imaging, Bulk-SPACE fundamental imaging, and SAW-SPACE fundamental imaging) could image significant portions of the samples provided by EDF. However, the linear and nonlinear images are often complementary suggesting that the cracks may be partly closed. For example, the fundamental component obtained with Bulk-SPACE images the open portions of the crack while the subharmonic component obtained with Bulk-SPACE images the closed portions of the crack. Moreover, the linear and nonlinear patterns are different (e.g. different shape, size and number of spots) which might be due to different physical mechanisms. The tip of the cracks for samples 2 and 3 could not be imaged with linear or nonlinear techniques and so no conclusion could be made as to whether the crack is closed near its tip.

3. Inspection Region of TREND

One of the previously unaddressed topics regarding the use of TREND as an inspection technique is that of the inspection region. Experimental work utilizing time reversal for nondestructive inspection typically employs out-of-plane foci on the surface of the sample. It is important to quantify the region of interrogation to allow near surficial feature imaging and depth estimation. We address this question here using numerical and experimental results.

3.1 Numerical Model Validation

In this section, elastic energy is focused near an edge of an aluminum sample. The adjacent side of the sample thus provides an experimental means of measuring a pseudo depth profile. The experimental data collected from this configuration are used to validate the numerical model.

Experiments were conducted on an aluminum sample with a rectangular shape and dimensions of $10\times10\times19$ cm^3. Figure 7 is a photograph of the experimental setup. Elastic energy was transmitted into the sample using eight identical piezoelectric disks (type PZT-5, diameter of 12.7 mm, and thickness of 2 mm) that were bonded onto three surfaces, at locations far from the desired focal point to allow diffusion of the elastic energy into the sample. The velocity wave field was measured on the surface of the sample using single point laser Doppler vibrometers (LDV) from Polytec Inc. A scanning system was developed that allows the laser vibrometer to record the motion of the sample at various locations within a region of interest with a system.

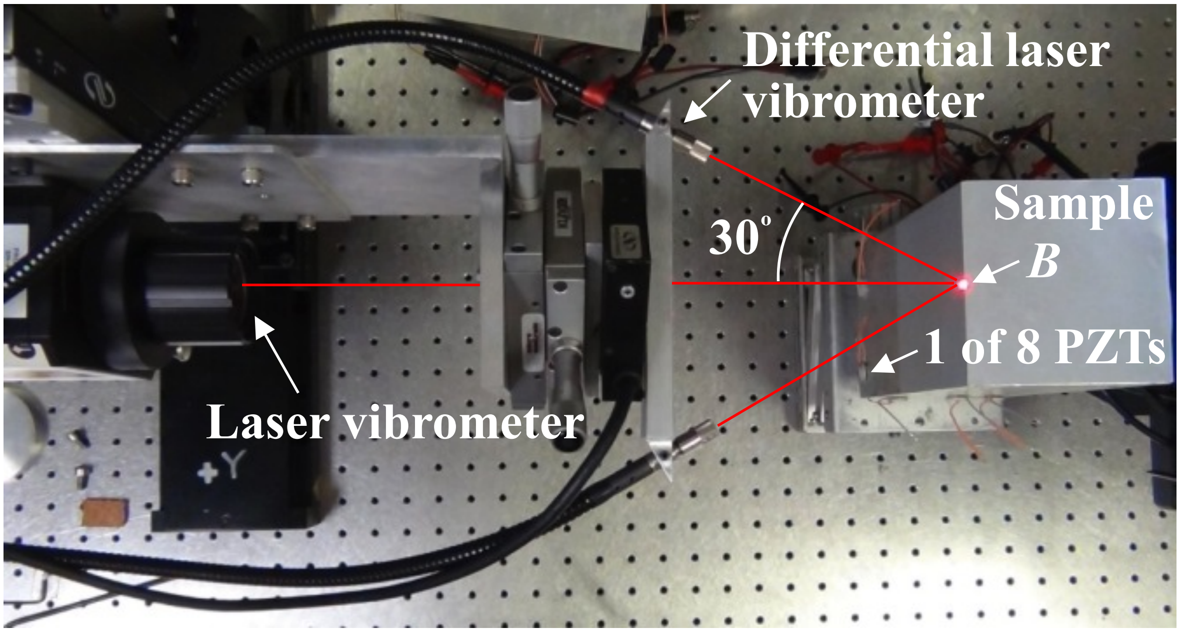

Figure 7. Photograph of the experimental setup used for validating the model used to quantify the inspection region of TREND.

The Reciprocal Time Reversal method [4] is used to create a focus of the vertical, in-plane component of motion centered at the location of the laser spot in Fig. 7 (point *B*). First, impulse responses (IRs) are determined between the PZT transducers and point *B*. For this purpose, a linear chirp signal with appropriate frequency bandwidth is emitted from a single PZT transducer while the vertical, in-plane velocity component is measured with the LDV at point *B*. This operation is repeated for all PZT transducers. Then, the IRs are determined from a cross correlation of the input chirp signal with the measured response, reversed in time, scaled in amplitude to maximize the amplifier output, and all reversed signals are broadcast simultaneously from the corresponding PZT transducers. This creates a TR focus of the vertical, in-plane velocity component (v_z). The in-plane velocity component (v_x) and the out-of-plane velocity component (v_y), are also measured. Spatial scans of the TR focus in each component of motion are displayed in Fig. 8.

The above experiment is simulated using the "Solid Mechanics" module of the commercial finite-element software package COMSOL MULTIPHYSICS 4.3a. The PZT transducers are modeled as normal surface loads applied at each transducer location. The time history of the surface load in the forward propagation step consists of a 50 kHz tone-burst, similar to that observed in the TR experiment at the focal point. The computational domain is discretized into tetrahedral elements with a maximum element size equal to a sixth of the smallest wavelength involved in the problem.

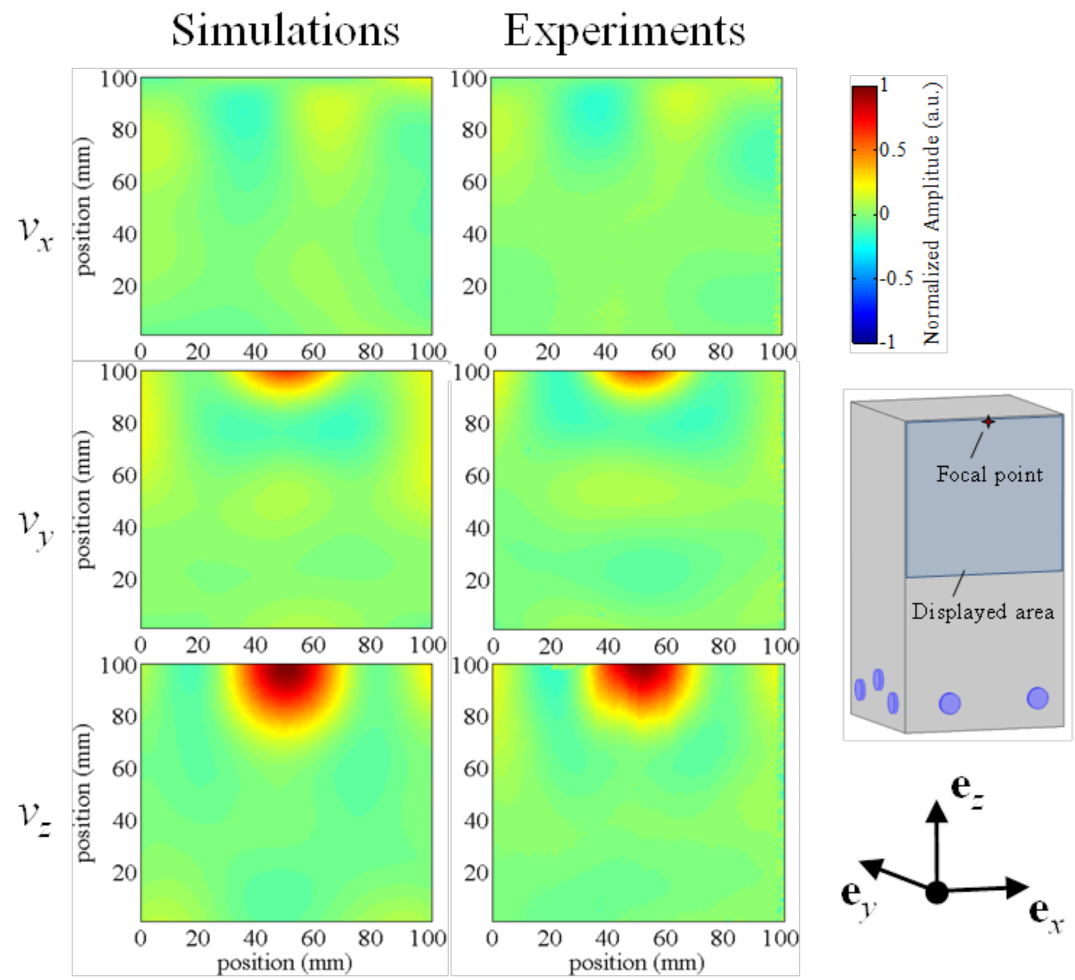

Figure 8. Velocity components at the focal time. Focusing was achieved using the v_z component at the focal point. The drawing on the right-hand side indicates the location of the focal point and the area on the sample surface where results are displayed. Simulated (left column) and experimental (right column) results. For each column, data are normalized with respect to the peak amplitude of v_z. The v_z signal generated at the focal point consists of a pulse centered at 52.8 kHz in simulations and at 54.7 kHz in experiments. As a result, the spot size of v_z is larger in simulations than in experiments. Notice the dipole motion around the focal point observed in v_x due to the Poisson effect. This motion has a much smaller amplitude than v_z at the focal point but is larger than the background.

Figure 8 depicts snapshots of the three simulated and measured velocity components, v_x, v_y, and v_z, at the focal time of $t = 1.876$ ms. Results are displayed on a portion of the surface surrounding the focal point. The v_z component exhibits the largest peak amplitude at the focal time, which is expected since this is the component used in the TR process. A significant portion of the energy is also contained in the y-component of the motion, as a result of focusing near an edge parallel to the x-axis. The asymmetry of the system in the y-direction (e.g. fluid or vacuum on one side of the focal point and solid on the other side) causes motion of the focal-point region in the y-z plane. Likewise, if the focal point was close to a corner of the sample, energy would be contained in all three components of the motion, regardless of the component used in the TR process, due to the asymmetry of the system in the three Cartesian directions. Last, it is interesting to observe the dipole structure of the v_x component around the focal point, due to the

Poisson effect. This motion has much smaller amplitude than v_z at the focal point but is larger than the background.

The numerical model captures successfully the main features of the elastic response observed in experiments, including the dipole structure of the v_x component and the focal spots for the v_y and v_z components in Fig. 8. Note that the size of the focal spot for the v_z component is larger in simulations than in experiments. The size of the focal spot is related to the center frequency of the refocused signal at the focal point. The signal of the v_z component at the focal point consists of a pulse centered at 52.8 kHz in simulations and 54.7 kHz in experiments, which implies a slightly smaller size of the focal spot in experiments. The close qualitative and quantitative agreements between experiments and simulations are remarkable given the different approaches used to create the TR signals.

3.2 Quantifying the Inspection Region

The out-of-plane velocity component (now v_z) is refocused numerically at the center of the top surface of the aluminum sample described in Section 3.1. Snapshots of the three simulated velocity components at the focal time are depicted in Fig. 9. Results are displayed on the top surface (x-y plane) and within the depth of the sample (x-z and y-z planes). As expected, the largest amplitude is observed for the v_z component while the in-plane components, v_x and v_y, exhibit the Poisson effect dipole structure discussed in Section 3.1. The shape of the focal spot is not perfectly symmetric with respect to the z-axis, indicating an imperfect reconstruction of the original source.

The diffraction limit is used here to find empirical relations between the size of the focal spot and the wavelengths (λ) of the P (compressional), S (shear), and R (Rayleigh) waves. From an analysis not presented here, it can be assumed that the size of the focal spot is controlled by the R waves on the surface of the sample and by the S waves in the bulk. The width and depth of the focal spot are measured at the half maximum value of the focused velocity component, in this case v_z. When focusing the out-of-plane motion component, the width is empirically expressed as,

$$w^{\mathrm{emp}} = \lambda_R / 2, \tag{1}$$

and the depth as,

$$d^{\mathrm{emp}} = 1.3\lambda_S / 4, \tag{2}$$

where the superscript “emp” refers to empirical.

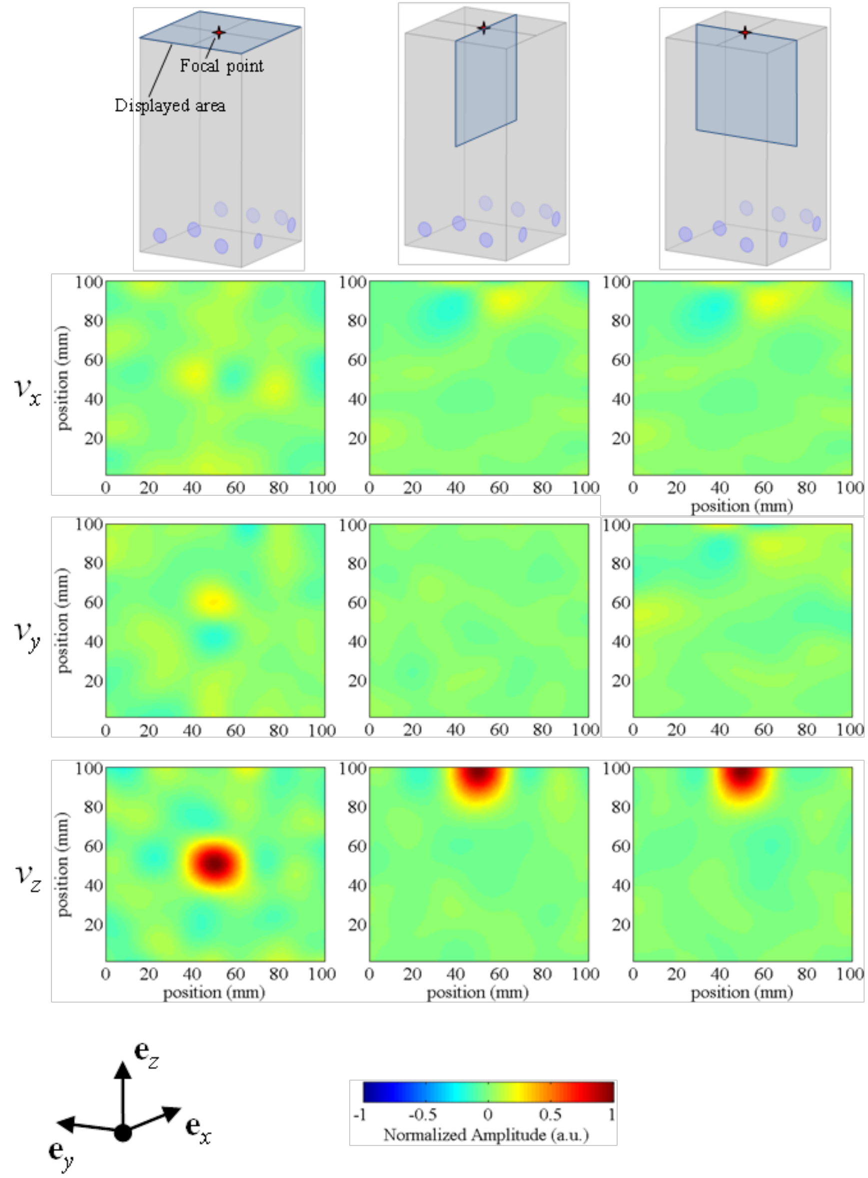

Figure 9. Simulated velocity components at the focal time. Focusing was achieved using the v_z component. The drawings on the bottom row indicate the location of the focal point and the area where results are displayed. Data are normalized with respect to the peak amplitude of v_z. The v_z signal generated at the focal point consists of a pulse centered at 79.2 kHz.

Simulations were also conducted on samples of varying material properties and with various center frequencies. Material properties were those of aluminum but with a Poisson ratio varied from 0.15 to 0.45. Center frequencies were varied from 53 to 169 kHz. There was a fair agreement between the observed and predicted sizes of the focal spots, with differences mostly within 5% for all cases considered. Besides the use of an empirical expression, variations of the results can be attributed to the imperfect reconstruction of the source in the time reversal process.

3.3 Summary of Inspection Region Study

This study quantified the size of the inspection region when time reversal is used to focus the out-of-plane velocity component on the surface of an isotropic solid sample for standard TREND measurements. The numerical model used in the analysis was first validated against experimental data. Subsequently, empirical expressions for the width and depth of the focal spot (that of the out-of-plane velocity component) were found based on (i) an interpretation of Lamb's problem [19] [20] to determine which waves dominate the propagation in the regions of interest (surface and bulk) and (ii) the use of the diffraction limit. In these expressions: the width of the focal spot depends only on the wavelength of the Rayleigh wave and the depth on the wavelength of the shear wave, at the center frequency of the refocused pulse. The empirical expressions were found to be robust to changes of the center frequency of the refocused pulse and of the Poisson ratio of the material.

4. Inspection of Concrete Structures

The work described here represents a collaboration between LANL, the Federal Institute for Material Research and Testing (Bundesanstalt für Materialforschung und –prüfung, in Berlin, Germany) and The Pennsylvania State University (State College, PA). The purpose of this project is to investigate the sensitivity of nonlinear acoustics based NDE techniques to the amount of microcracking in concrete. The objective is to assess the capability of various linear and non-linear measures in discriminating structurally-sound concrete from that with distributed micro-damage. A number of damage mechanisms in concrete result in distributed microcracking at the initial or advanced stages of development. Thermal and mechanical damage processes are two of the better-understood damage processes of this type. The potential of nonlinear-acoustics based NDE in characterizing thermally induced damage in concrete has been explored in [21]. We have studied the sensitivity of various linear and nonlinear acoustic measures to mechanical (stress-induced) damage here. The following is a description of the samples and of the main results of this project available at the time of this report.

The preliminary ultrasonic testing and loading of the specimens took place at Germany's Federal Institute for Materials Research and Testing (BAM) located in Berlin, Germany. The intact specimen B1 and the damaged ones (B2 to B8) were soon after shipped to LANL. At LANL a series of linear and nonlinear measurements were conducted on these specimens. This included: RUS (Resonant Ultrasound Spectroscopy), NRUS (Nonlinear Resonant Ultrasound Spectroscopy), variable amplitude continuous wave measurements required for SSM (Scaling Subtraction Method) and DAET (Dynamic Acousto-elasticity Testing).

4.1 Samples

Eight prismatic concrete samples of the same nominal size were cut out of a relatively large (approx. 300 x 300 x 500 mm^3) concrete block. All the samples have a rectangular 50 mm x 50 mm cross-section and are 150 mm long. Since the samples were cut out of an existing concrete mass, we do not have the exact mix characteristics, however, visual inspection of the samples indicates that the largest aggregate size is about 20 mm, thus representing a typical concrete mix used in construction. The samples have an average mass density of about 2302.7 kg/m^3 with a standard deviation of less than 16 kg/m^3. After cutting the eight (8) samples, we arbitrarily labeled them B1 to B8, where B stands for 'Beton', meaning concrete in German.

4.2 Initial Linear Measurements

Prior to inducing mechanical damage, (linear) ultrasonic wave velocities were measured in all samples. We measured the wave velocities along the length (i.e., the largest dimension) of each sample in a transmission mode, employing two broadband P-wave transducers of a center frequency of about 200 kHz. An Agilent 33120A arbitrary waveform generator was used to broadcast Mexican hat pulses of center frequencies ranging from 50 to 250 kHz in 50 kHz steps, as well as rectangular pulses centered at 50, 100, and 150 kHz. Following the measurements, wave velocities were measured from the time-of-flight (TOF) using a handful of criteria such as picking the arrival of the first maxima, the first minima, reaching a certain threshold, etc. All different methods yielded similar results. The average velocities obtained by picking the arrival of the first maximum when using a Mexican hat pulse had a linear velocity variation among the different samples of less than 4%. Given that the typical level of uncertainty in such measurements is known to be about 5%, we can argue that linear ultrasonic velocity measurements would not be able to differentiate one sample from the other. The velocity measurements on B4 were anomalous and thus the results obtained on this specimen are excluded from most of our further processing.

The measured ultrasonic wave velocities are slightly dispersive (i.e., speed of sound varies with frequency). We observe a monotonic increase of velocities for all the samples when the frequency is increasing from 100 to 250 kHz. This observation is consistent with the simulated/measured ultrasonic velocity dispersion characteristics in stochastic regime in heterogeneous media reported by others.

4.3 Inducing Mechanical Damage

After taking the initial linear measurements, the specimens were individually placed in a MTS loading machine and compressed to various load levels to induce various degrees of mechanical damage. To obtain the ultimate compressive strength (i.e., maximum stress at failure) of the samples, one of the samples (B2) was arbitrarily chosen and pressed until failure. A maximum compressive stress of 51 MPa for this sample. Having obtained the maximum load for B2, the other specimens were compressed to various percentages of this maximum load. B1 was left unloaded to serve as the intact reference specimen. B3, B4, B5, B6, B7 and B8 were loaded up to 10%, 20%, 30%, 40%, 60% and 70% of the maximum load for B2, 127.5 kN or 51 MPa, respectively. The various percentages were chosen in an attempt to induce different levels of micro-damage in concrete.

To understand the stress-induced damage at various stress levels, it is worthwhile to study the stress-strain behavior of concrete under uniaxial compression. A typical stress-strain curve for plain concrete subjected to monotonically increasing strain (strain-controlled) is shown in Fig. 10. Both axes are normalized; the stress on the vertical axis is normalized with respect to the maximum stress after which the strain rapidly increases without any additional increase in stress (51 MPa for B2), the strain on the horizontal axis is normalized by the strain at the maximum stress, which ranges from 0.002 to 0.003 for normal density concrete mixes. Mehta and Monteiro [22] have outlined the typical stress-strain characteristics of concrete as follows:

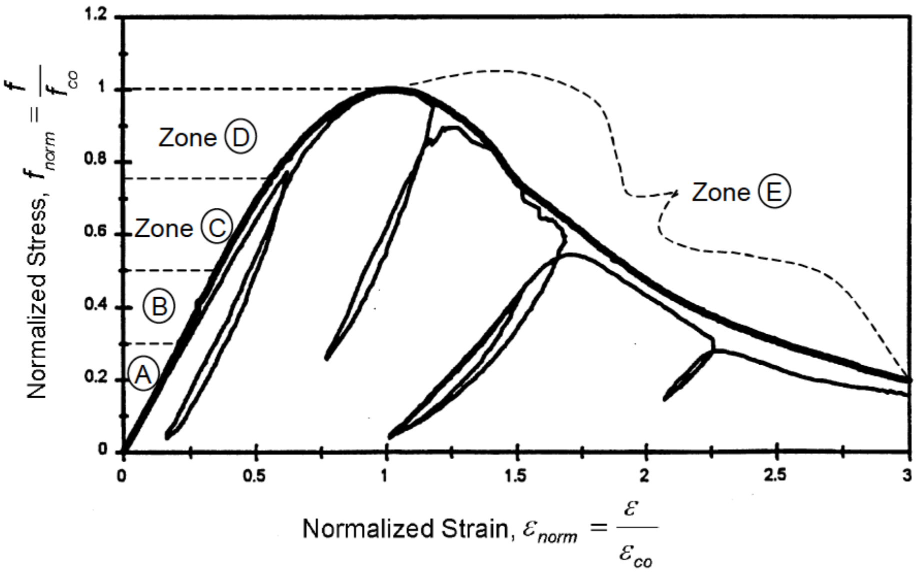

Figure 10. Typical monotonic stress-strain curve and cyclic envelope curve for plain concrete (from [23].)

1. Zone A: concrete exhibits a linear-elastic response under compressive stresses less than about 30% of the compressive strength. The crack initiation and growth is minimal, stable (i.e., does not continue to grow under constant loading) and largely limited to the aggregate-cement interface zone.
2. Zone B: a significant increase in crack initiation and growth in the interfacial zone is expected for stress ratios between 30% and 50%. However, the crack growth is expected to remain stable.
3. Zone C: for stress ratios between 50% and 75%, the crack initiation and growth are gradually spread to the cement matrix. The crack growth may be unstable.
4. Zone D: for stress ratios greater than 75%, the micro-cracking initiation and growth accelerates in the interfacial zone as well as cement paste. Moreover, small micro-cracks coalesce to form continuous cracks.
5. Zone E: loading concrete to compressive strains beyond the maximum results in the development of more and more continuous cracks and ultimate failure of the specimen.

The loading levels were chosen such that specimens B3 and B4 fall in Zone A. Specimens B5 and B6 in Zone B and specimens B7 and B8 in Zone C. No specimen was loaded beyond 70%, because such level of damage results in a significant drop in material stiffness and the damage is easily characterized by (among others) standardized linear acoustic measurements. Therefore, no apparatus of higher sensitivity would be required.

4.4 Linear Measurements on Damaged Samples

We measured the linear ultrasonic wave velocities for the eight (8) damaged specimens. We followed the very same test protocol as described above. Damage due to stresses as high as 70% of the maximum compressive strength alter the linear wave velocities by no more than 6%. The velocities are *generally* decreasing with the increasing stress-strength ratio. However, the changes are within the level of uncertainty in such measurements (about 5%). In other words, linear measurements fail to reliably differentiate between the intact sample and that pressed to about 70% of its compressive strength.

4.5 Resonant Ultrasound Spectroscopy (RUS)

Resonant ultrasound spectroscopy (RUS) is a vibration-based laboratory technique, which can yield the complete elastic tensor of a piece of material [24]. RUS involves obtaining a number of mechanical vibration modes of a sample supported at only a few single points by sweeping the frequency across a certain range. The frequency sweep is typically repeated a few times, changing the transducer and support locations. Having recorded a sufficient number of modal peaks, one can back-calculate the elastic moduli knowing the sample's exact geometry and density.

RUS was performed on all 8 specimens using Resonance Inspection Techniques and Analyses (RITA) [25], a data acquisition system developed at LANL; we carefully measured the specimen dimensions and their densities (ρ). For each specimen, ten (10) modal frequencies were measured ranging between 5 kHz and 25 kHz. Assuming a homogenized linear elastic material model, the Young's and shear moduli (C_{11} and C_{44}) were calculated using the Visscher algorithm as described in [24]. The measured elastic constants along with the dimensions and densities for all the specimens are summarized in Table 4 below. The last two columns in this table are the corresponding estimations of compressional wave (or P-wave) V_P and shear wave (S-wave) velocity V_S , obtained as follows:

$$V_P = \sqrt{c_{11}/\rho}\,,\ V_S = \sqrt{c_{44}/\rho}\,. \tag{1}$$

Table 4. RUS summary results.

	Damage	Dimensions (cm^3)	C11=C22=C33	C44=C55=C66	Density (gm/cc)	Vp (m/s)	Vs (m/s)
B1	0%	4.98x4.99x15.20	0.33111	0.15272	2.289	3803	2583
B2	100%	5.02x5.03x15.00	0.21988	0.09366	2.332	3071	2004
B3	10%	4.98x5.00x15.20	0.31085	0.15127	2.283	3690	2574
B4	20%	5.00x4.99x15.20	0.28469	0.1387	2.287	3528	2463
B5	30%	5.01x5.00x15.10	0.30241	0.14447	2.3	3626	2506
B6	40%	5.01x4.99x15.10	0.29962	0.14128	2.302	3608	2477
B7	60%	5.00x5.01x15.10	0.36577	0.15849	2.319	3971	2614
B8	70%	5.01x5.02x15.10	0.33304	0.1415	2.31	3797	2475

A comparison of RUS-based V_P (as obtained in Eq. 1) measured at LANL and the ultrasonic wave velocities measured at 100 kHz at BAM for all eight specimens show that, although measured at very different frequencies, the velocities are in a very good agreement, except for

B2. Having been measured at a much lower frequencies, the RUS-based velocities are generally slightly lower than the ultrasonic velocities.

4.6 Nonlinear Resonant Ultrasound Spectroscopy (NRUS)

For the NRUS measurements, a thick piezoelectric ceramic element is mounted on one side of each specimen. The frequency is swept over a frequency range containing one or more of the selected vibration modes. After completion of one frequency sweep, the input voltage to the piezoelectric element is increased. At higher amplitudes, the resonance frequencies will be shifted towards lower frequencies for nonlinear materials. The higher the amplitude, the larger is the relative shift of the resonance frequencies. Nonlinear parameter alpha (α) is the relative shift in resonance frequency (w.r.t. the linear resonance frequency or the resonance frequency at low excitation amplitudes) per unit strain. Highly nonlinear materials (with classical nonlinearity) are characterized with large values of α. Thermal damage in cement and microcracking in bones have shown to result in an increase in α.

NRUS was conducted on all the samples except for B2 and B4, which are excessively damaged. The first compressional mode was used to calculate the relative shift in resonance frequency. We used numerical modeling (COMSOL) to help choose the target mode (Fig. 11). The transducer (including the double-element arrangements and the steel back load) was included in the model. In an NRUS spectrum, the mode was selected which had the closest frequency to the frequency of the pure compressional mode of the modeled specimen-transducer assembly.

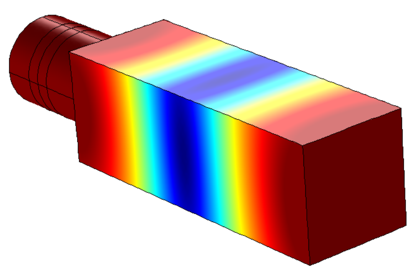

Figure 11. Numerical modeling was used to determine the first compressional mode.

The obtained relative shift in the resonance frequencies versus strain for all the tested specimens are shown in Fig. 12(a). The corresponding values for the nonlinear parameter α are given in Fig. 12(b). The frequency shift for damaged specimens is significantly greater than that for the undamaged specimen (B1) at the same strain level. For example, at the strain of 2.5e–6, the relative frequency shift for B1 is about –0.002, while it is –0.007 for B8. Consequently, α for B8 is more than three times larger than that for B1. In other words, the two specimens are clearly distinguishable in terms of their nonlinear parameter alpha. The values for the other specimens fall in between. Since the actual amount of volumetric microcracking in the specimens is not known, further conclusions about the correspondence of the test results and the level of microcracking cannot be drawn.

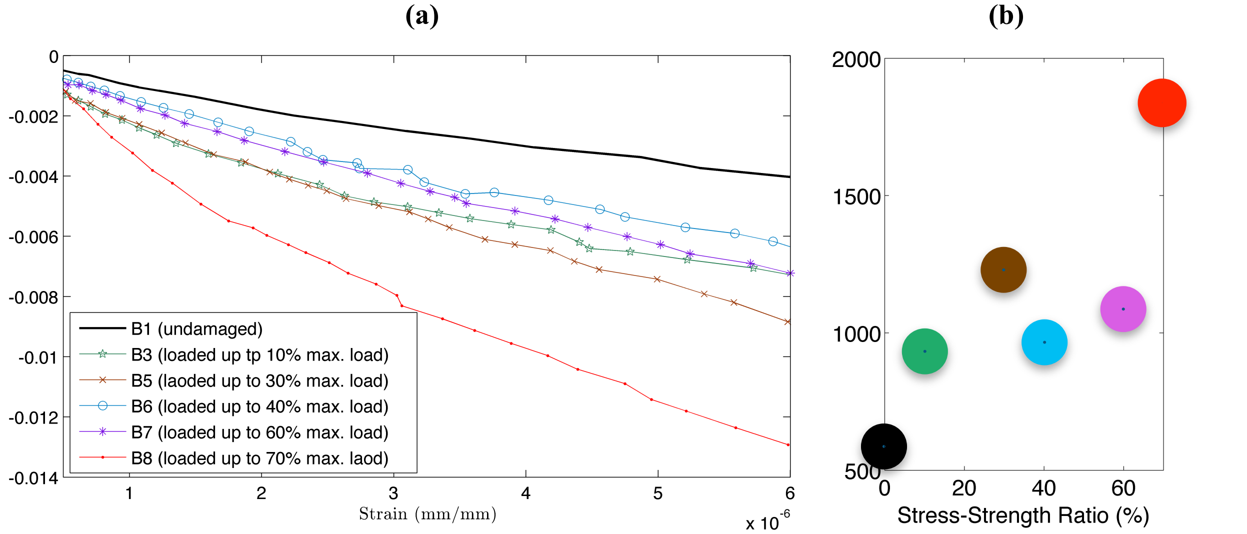

Figure 12. Relative change of resonance frequency for B1, B3, B5, B6, B7 and B8. (a) Frequency shift with respect to strain amplitude. (b) Nonlinearity as a function as a function of damage level (i.e., max loading with respect to compressive strength.)

4.7 Dynamic Acousto-Elasticity Testing (DAET)

In this section, the results of DAET on two specimens with the least and most damage are discussed. We chose these two specimens, because they are not differentiable by visual inspection and their difference is not practically measurable in terms of linear ultrasonic velocities or elastic moduli as obtained by RUS. Nevertheless, B8 was pressed to 70% of the maximum load at failure of B2, indicating a significant amount of micro-cracking. Therefore, it is safe to assume that we are comparing here two specimens with low (or minimal) and high density of volumetric micro-cracks, which we could not previously delineate using any of the linear acoustic techniques employed.

The DAET setup utilized large piezoelectric ceramic elements of 2 in. diameter and ¼ in. thickness for low-frequency excitation of the samples. A pair of high-frequency Olympus transducers with a center frequency of 1 MHz was used to probe the changes in response to the low-frequency modulating excitation in four different configurations. The test protocol was as follows. First, the velocities were measured using the high-frequency transducers in the absence of low-frequency modulation. After about 40 acquisitions, the low-frequency "pump" was turned on. The frequency of the pump was chosen to be close to the first compressional mode of the specimen. This ensures high-amplitude excitation. Throughout the test, the low-frequency vibrations were monitored using a small accelerometer mounted on top of the specimen. While the pump is on, the high-frequency transducers monitored the local changes in the medium. After about 400 acquisitions, the pump (i.e., low-frequency excitation) was turned off, while the high-frequency transducers continued to probe the local changes in the specimen for another 1000 acquisition cycles. This final step was aimed at studying slow dynamics or the characteristics of the recovery of the changes in the specimen after removing the low-frequency excitation source.

Unlike typical DAET measurements, longer high-frequency records (0.2 ms) were taken here to study the effect of the low-frequency excitation on the diffuse ultrasonic waves in concrete. Coda wave interferometry (CWI) was used to measure the changes in velocities. CWI is a cross-correlation based technique, which enables the accurate detection of subtle changes in velocities in a perturbed medium. The evolutions of velocities during the experiment at a strain level of about 5e-5 for B1 and B8 are shown in Fig. 13.

Figure 13. Relative change in velocity in (a) B1 (undamaged) and (b) B8 (damaged) sample at a pump-strain of approximately 5e-5.

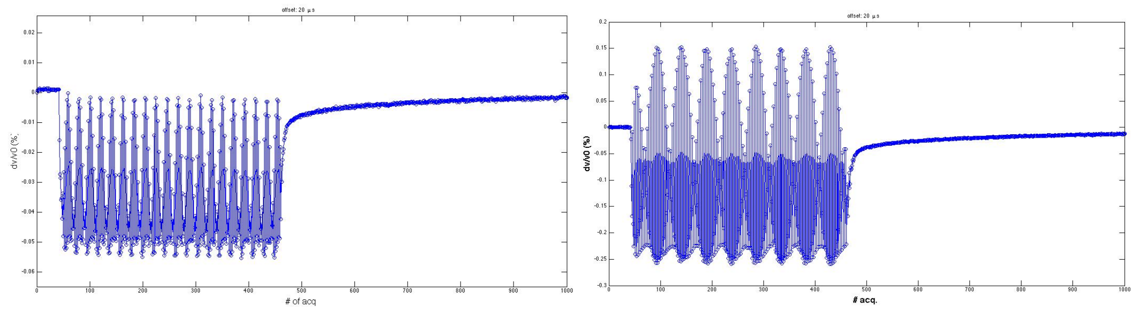

(a) **(b)**

The velocity changes for B8 (varying between +0.15% and –0.25%) are about eight (8) times higher than those measured for B1 (varying between 0 and –0.05%). The rate of recovery of velocities after turning off the modulating low frequency excitation is also noticeably different for the two specimens; while the velocities for B8 are still recovering, those measured for B1 are almost recovered to the original values after 1000 acquisitions. Greater changes in velocities and slower rate of recovery in B8 indicate the presence of volumetric microcracks. In another words, the two specimens can be clearly distinguished using DAET measurements.

4.8 Concrete Work Summary

It is clearly demonstrated that nonlinear acoustics-based techniques are capable of delineating concrete specimens with and without moderate levels of volumetric stress-induced micro-damage. While linear ultrasonic measurements and RUS could not distinguish the undamaged and most damaged specimens in the series, the difference between these two specimens was obvious in all nonlinear-acoustics based measurements. *In particular, synergic combination of coda wave interferometry and DAET seems to provide a highly sensitive tool for micro-damage detection.* However, nonlinear-acoustics based measurements are highly sensitive to the quality of bonding between the transducers and specimens and no standard procedures for their application to concrete yet exists. Comprehensive investigations aimed at correlating the density of micro-cracks to the measured macroscopic parameters are needed to allow quantification of the micro-damage.

5. Conclusions

The 1st study on the collaborative effort to study SCC analogs (artificially generated closed cracks) is an ongoing study. It is very difficult to obtain an actual SCC sample or to create a sample with a closed crack. The samples provided by Trueflaw, by way of EDF, showed some signs of a closed crack behavior but the results were not conclusive. Further testing is planned at LANL to study these samples and to create better ones. Bulk-SPACE and SAW-SPACE were both used to image the nonlinear acoustic signature of closed portions of the crack. Despite the assertion by Trueflaw, a company that specializes in the manufacturing of closed crack samples, the cracks were partially open because they could be imaged with linear acoustic techniques and only partially imaged with nonlinear acoustic techniques, suggesting that they did not have large portions that were closed.

The 2nd study on quantifying the inspection region for a single time reversal focus of energy used in TREND experiments determined that the surficial extent (diffraction limit) of the focus is half of the Rayleigh wavelength and that the depth (diffraction limit) of the focus is one third the shear wavelength. Thus lower frequencies (larger wavelengths) should penetrate deeper below the surface to allow deeper inspection below the surface. However, lower frequencies result in a larger inspection region at the surface and therefore lower spatial resolution. Higher frequencies (smaller wavelengths) on the other hand, will not penetrate much into the sample, but they will yield a higher spatial resolution on the surface. These conclusions will hold irrespective of the type of material being inspected.

The 3rd study on applying nonlinear acoustics to inspection the damage state of concrete found that the linear inspection techniques could not distinguish the damage state of the concrete sample, despite the sample undergoing a compressive stress of 70% to failure. Fortunately, each of the nonlinear techniques applied, including TREND and DAET, were able to clearly distinguish whether the concrete was damaged or not.

The work contained herein will be prepared for peer review. Additional studies on SCC [26], fatigue cracks [27], and concrete degradation [28] inspections using nonlinear ultrasonic techniques appear in the peer-reviewed literature, and thus were not contained in this report.

6. References

[1] R Parrott and H Pitts, "Chloride stress corrosion cracking in austenitic stainless steel," 2011.

[2] J. A. Ten Cate, T. J. Ulrich, and N. R. Brown, "Corrosion and stress corrosion cracking: Recommendations for mitigation and advanced detection," 2012.

[3] Robert A. Guyer and Paul A. Johnson, *Nonlinear Mesoscopic Elasticity*, 1st ed. Berlin, Germany: Wiley VCH, 2009.

[4] Brian E. Anderson, Michele Griffa, Carene Larmat, T. J. Ulrich, and Paul A. Johnson, "Time reversal," *Acoustics Today*, vol. 4, no. 1, pp. 5-16, Jan. 2008.

[5] V. V. Kazakov, A. Sutin, and P. A. Johnson, "Sensitive imaging of an elastic nonlinear wave source in a solid," *Applied Physics Letters*, vol. 81, no. 4, pp. 646-648, 2002.

[6] T. J. Ulrich, A. M. Sutin, R. A. Guyer, and P. A. Johnson, "Time reversal and nonlinear elastic wave spectroscopy TR NEWS techniques," *International Journal of Nonlinear Mechanics*, vol. 43, pp. 209-216, 2008.

[7] T. J. Ulrich et al., "The time reversed elastic nonlinearity diagnostic applied to evaluation of diffusion bonds," *Applied Physics Letters*, vol. 93, p. 151914, 2008.

[8] T. J. Ulrich, P. A. Johnson, and A. M. Sutin, "Imaging nonlinear scatterers applying the time reversal

mirror," *J. Acoust. Soc. Am.*, vol. 119, pp. 1514-1518, 2006.

[9] M. Scalerandi, A. S. Gliozzi, L. E. Bruno, and K. Van Den Abeele, "Nonlinear acoustic time reversal imaging using the scaling subtraction method," *Journal of Physics D: Applied Physics*, vol. 41, p. 215404, 2008.

[10] V. M. Albers, *Underwater Acoustics Handbook II*. State College, PA: The Pennsylvania State University Press, 1965.

[11] B. E. Anderson, B. Moser, and K. L. Gee, "Loudspeaker line array educational demonstration," *Journal of the Acoustical Society of America*, vol. 131, no. 3, pp. 2394-2400, 2012.

[12] Y. Ohara et al., "Imaging of closed cracks using nonlinear response of elastic waves at subharmonic frequency ," *Applied Physics Letters*, vol. 90, no. 1, p. 011902, 2007.

[13] Y. Ohara, S. Horinouchi, M. Hashimoto, Y. Shintaku, and K. Yamanaka, "Nonlinear ultrasonic imaging method for closed cracks using subtraction of responses at different external loads," *Ultrasonics*, vol. 51, no. 6, pp. 661-666, 2011.

[14] S. Horinouchi, M. Ikeuchi, Y. Shintaku, Y. Ohara, and K. Yamanaka, "Evaluation of closed stress corrosion cracks in Ni-based alloy weld metal using subharmonic phased array," *Japanese Journal of Applied Physics*, vol. 51, p. 07GB15, 2012.

[15] Trueflaw LTD., "www.trueflaw.com," Espoo, Finland, 2014.

[16] O. Bou Matar, Y. F. Li, and K. Van Den Abeele, "On the use of a chaotic cavity transducer in nonlinear elastic imaging," *Applied Physics Letters*, vol. 95, p. 141913, 2009.

[17] B. Van Damme, K. Van Den Abeele, and O. Bou Matar, "The vibration dipole: A time reversed acoustics scheme for the experimental localisation of surface breaking cracks," *Applied Physics Letters*, vol. 100, no. 8, p. 084103, 2012.

[18] T. J. Ulrich et al., "Three component time reversal: Focusing vector components using a scalar source," *Journal of Applied Physics*, vol. 106, no. 11, p. 113504, 2009.

[19] H. Lamb, "On the propagation of tremors over the surface of an elastic solid," *Philosophical Transactions of the Royal Society of London*, vol. A203, pp. 1-42, 1904.

[20] J. D. Achenbach, *Wave Propagation in Elastic Solids*. Amsterdam: Elsevier Science, 1973.

[21] C. Payan, T. J. Ulrich, P.-Y. Le Bas, T. Saleh, and M. Guimaraes, "Quantitative linear and nonlinear resonance inspection techniques and analysis for material characterization: Application to concrete thermal damage," in *Acoustics 2012 Proceedings*, Hong Kong, China, 2012.

[22] P. Kumar Mehta and Paulo J. M. Monteiro, *Concrete: Microstructure, Properties, and Materials*, 3rd ed.: Prentice Hall, 1993.

[23] Bahn and Hsu, "Stress-strain behavior of concrete under cyclic loading," *ACI Materials*, vol. 95, pp. 178-193, March-April 1998.

[24] Albert Migliori and John Sarrao, *Resonant Ultrasound Spectroscopy: Applications to Physics, Materials Measurements and Nondestructive Evaluation*, 1st ed.: J. Wiley, 1997.

[25] T. J. Ulrich and Pierre-Yves Le Bas. (2010) Resonance Inspection Techniques and Analyses, LA-CC-10-108. Software.

[26] Sylvain Haupert, Brian E. Anderson, Yoshikazu Ohara, Timothy J. Ulrich, and Paul A. Johnson, "Optimized dynamic acousto-elasticity applied to fatigue damage and stress-corrosion cracking," *Journal of Nondestructive Evaluaion*, January 2014.

[27] Jacques Riviere et al., "Dynamic Acousto-Elasticity in a closed fatigue-cracked sample," *Journal of Nondestructive Evaluation*, February 2014.

[28] Cedric Payan et al., "Probing material nonlinearity at various depths by the use of time reversal mirror and focal time delay analysis," *Applied Physics Letters*, 2014.